Supporting Information

Enhancing CO$_2$/N$_2$ and CH$_4$/N$_2$ separation performance by salt-modified aluminum-based metal-organic frameworks

Peng Zhang, Sai Ma, Yujuan Zhang, Chaohui He*, Tuoping Hu*

Department of Chemistry, College of Chemistry and Chemical Engineering, North University of China, Taiyuan, 030051, Shanxi, P. R. China

Corresponding authors E-mail: hechaohui0076@163.com; hutuoping@nuc.edu.cn

Isosteric heat of adsorption

The adsorption heat for CO_2, CH_4 and N_2 on MOF-253, MOF-253@Cu(BF$_4$)$_2$, MOF-253@Zn(BF$_4$)$_2$ and MOF-253@ZnSiF$_6$ were calculated using the Clausius-Clapeyron equation as follows:

$$Q_{st} = RT^2 \left(\frac{\partial \ln p}{\partial T} \right)_q$$

where Q_{st} represents the adsorption heat (kJ/mol), P is the pressure (kPa), T represents the temperature (K), R is a constant and q represents the adsorption amount (mmol/g).

Ideal adsorbed solution theory (IAST) calculations

The single-component adsorption isotherms of CO_2, CH_4 and N_2 on MOF-253, MOF-253@Cu(BF$_4$)$_2$, MOF-253@Zn(BF$_4$)$_2$ and MOF-253@ZnSiF$_6$ obtained at 298 K were fitted using the dual site Langmuir-Freundlich model.

$$q = q_{A,sat} \frac{b_A p^{v_A}}{1 + b_A p^{v_A}} + q_{B,sat} \frac{b_B p^{v_B}}{1 + b_B p^{v_B}}$$

where q represents the adsorbed capacity per mass of adsorbent (mol/kg), $q_{A,sat}$ and $q_{B,sat}$ are the saturation uptake capacities at site A and site B, respectively, b_A and b_B represent the constant at adsorption site A and site B, respectively, P represents the total pressure of the gas at the equilibrium (kPa) and v represents the Freundlich exponent.

The adsorption selectivity defined as follows:

$$S_{ads} = \frac{q_A / q_B}{y_A / y_B}$$

where q_A and q_B represent the component molar loading within the MOFs and y_A and y_B are the corresponding mole fraction used in the feed gas mixture.

Density-functional theory (DFT) calculations

The binding sites for CO_2 and CH_4 in MOF-253@ZnSiF$_6$ were identified using DFT calculations. This task is accomplished using the Quantum-Espresso package in Material Studio software. In order to explain the Van der Waals interactions, the dispersive forces (semi-empirical) were added to the traditional DFT in the calculation. The crystal structure of MOF-253@ZnSiF$_6$ was first optimized and CO_2 or CH_4 were then introduced at different positions in the MOF structure with adequate relaxation.
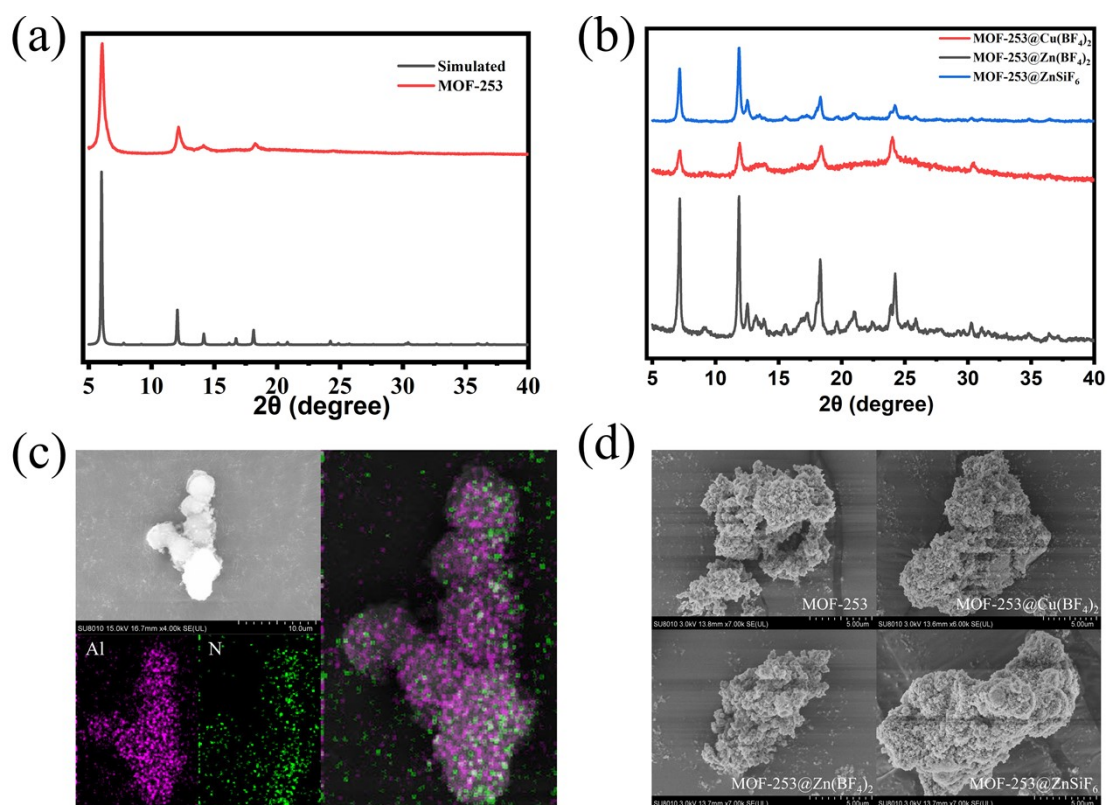
Fig. S1. (a) PXRD patterns recorded for MOF-253; (b) PXRD patterns recorded for MOF-253@Cu(BF$_4$)$_2$, MOF-253@Zn(BF$_4$)$_2$ and MOF-253@ZnSiF$_6$ (c) SEM and EDS images of MOF-253; (d) SEM images of MOF-253, MOF-253@Cu(BF$_4$)$_2$, MOF-253@Zn(BF$_4$)$_2$ and MOF-253@ZnSiF$_6$.
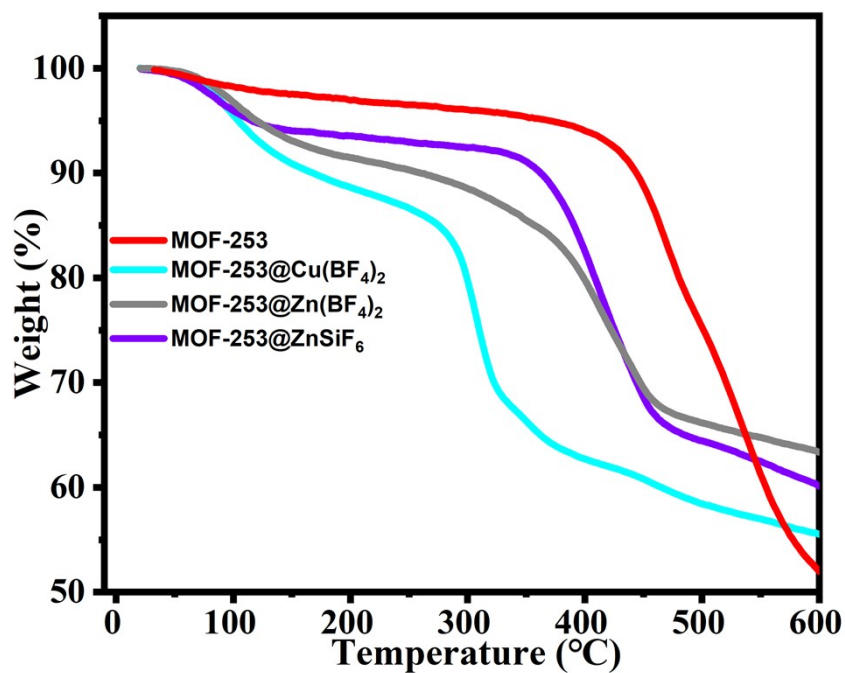
Fig. S2. TGA curves of MOF-253, MOF-253@Cu(BF$_4$)$_2$, MOF-253@Zn(BF$_4$)$_2$ and MOF-253@ZnSiF$_6$.
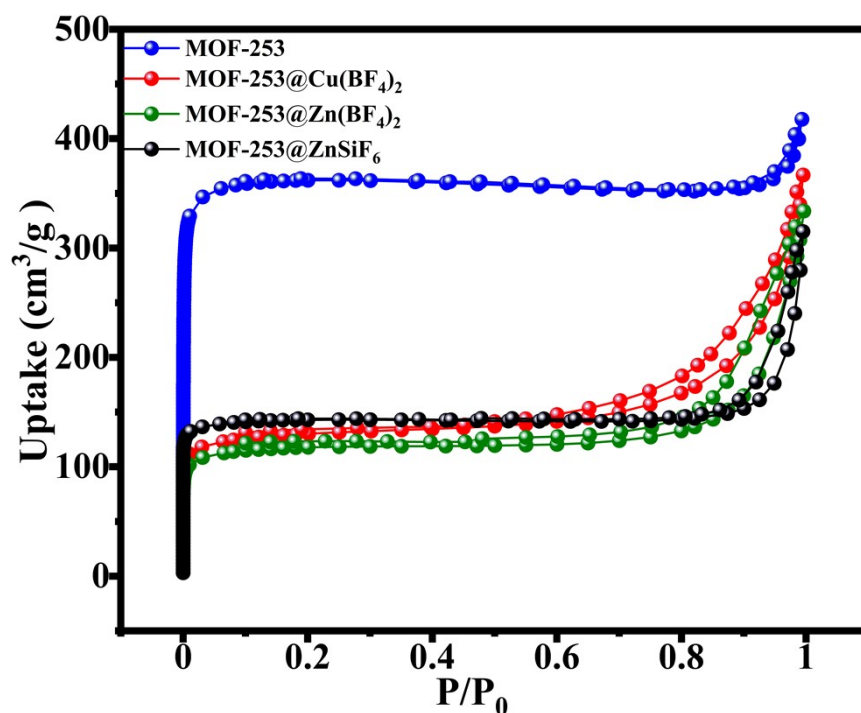
Fig. S3. N$_2$ adsorption-desorption isotherms of MOF-253, MOF-253@Cu(BF$_4$)$_2$, MOF-253@Zn(BF$_4$)$_2$ and MOF-253@ZnSiF$_6$ at 77 K.
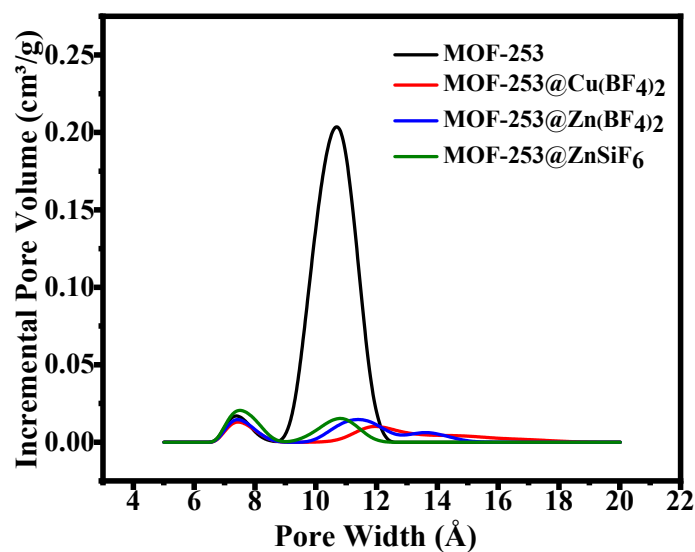
Fig. S4. The pore size distributions of MOF-253, MOF-253@Cu(BF$_4$)$_2$, MOF-253@Zn(BF$_4$)$_2$ and MOF-253@ZnSiF$_6$ obtained by DFT method.
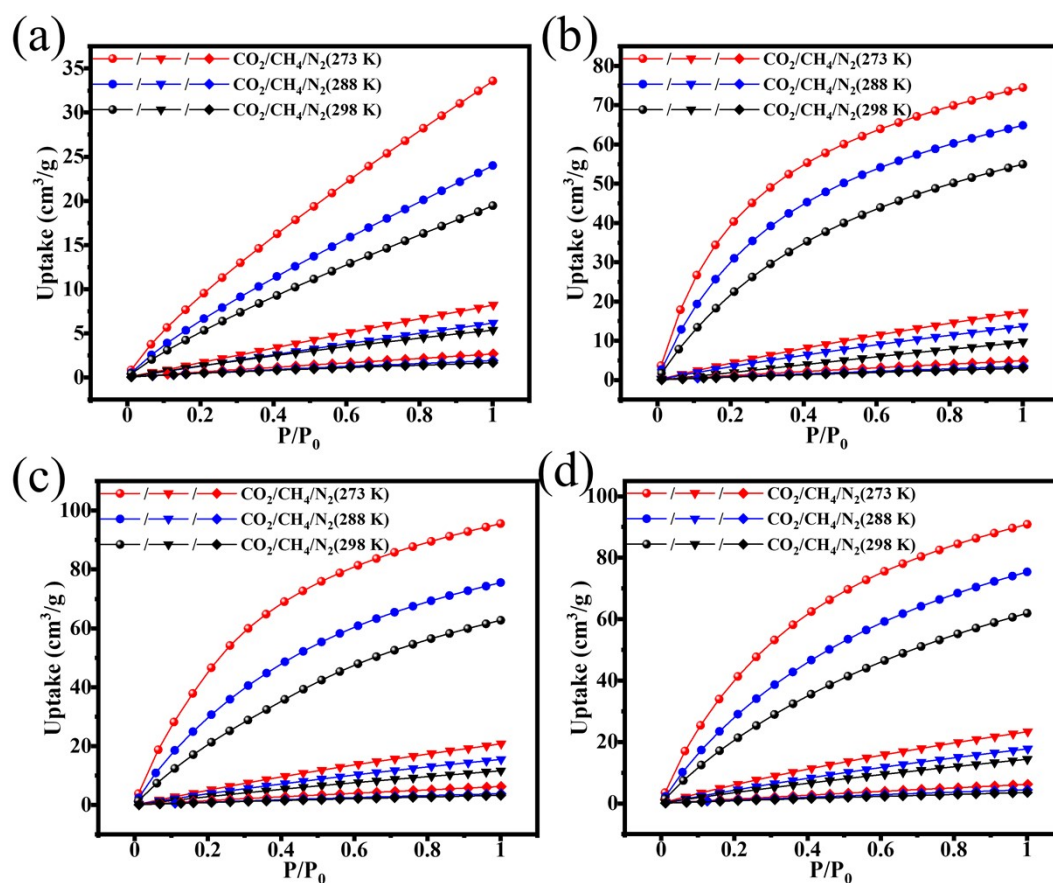
Fig. S5. The single-adsorption isotherms of (a) MOF-253, (b) MOF-253@Cu(BF$_4$)$_2$, (c) MOF-253@Zn(BF$_4$)$_2$ and (d) MOF-253@ZnSiF$_6$ for CO$_2$, CH$_4$ and N$_2$ at 273, 288 and 298 K.
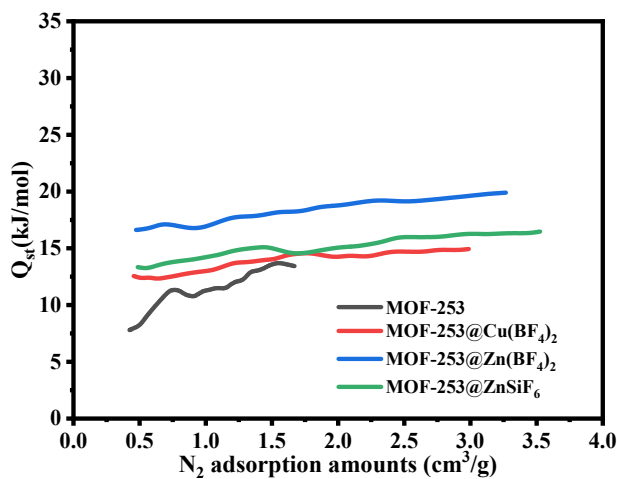
Fig. S6. The adsorption heat of MOF-253, MOF-253@Cu(BF$_4$)$_2$, MOF-253@Zn(BF$_4$)$_2$ and MOF-253@ZnSiF$_6$ for N$_2$.
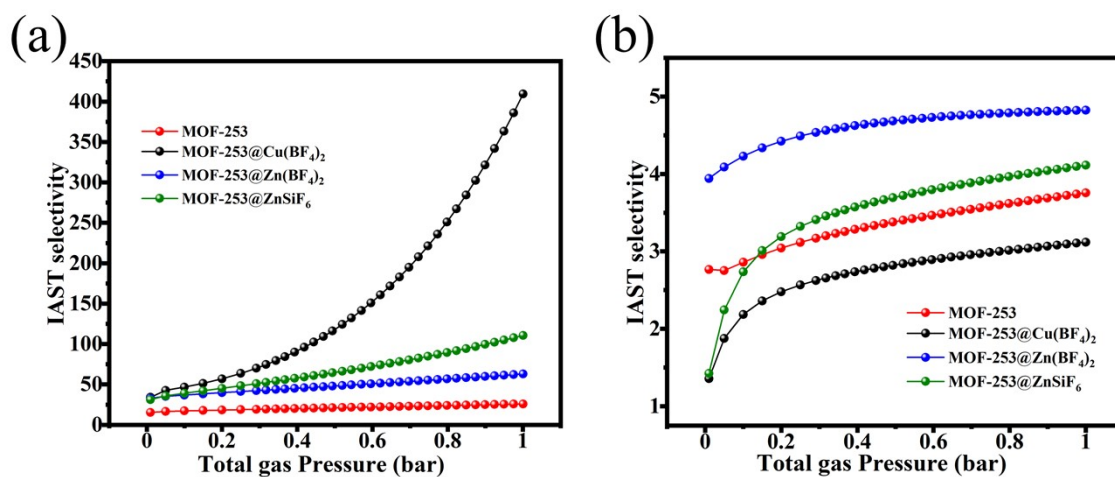
Fig. S7. The adsorption selectivity of (a) CO$_2$/N$_2$ (1/1, v/v) and (b) CH$_4$/N$_2$ (1/1, v/v) for MOF-253, MOF-253@Cu(BF$_4$)$_2$, MOF-253@Zn(BF$_4$)$_2$ and MOF-253@ZnSiF$_6$ at 298 K.

Fig. S8. The breakthrough experimental set-up schematic.

Fig. S9. PXRD patterns of MOF-253@ZnSiF$_6$ treated at different conditions.

Fig. S10. CO_2, CH_4, and N_2 adsorption isotherms at 298 K in a series of salt-modified MOF-253 with dual-site Langmuir-Freundlich model fits.

Table S1 Physicochemical properties of CO_2, CH_4 and N_2.

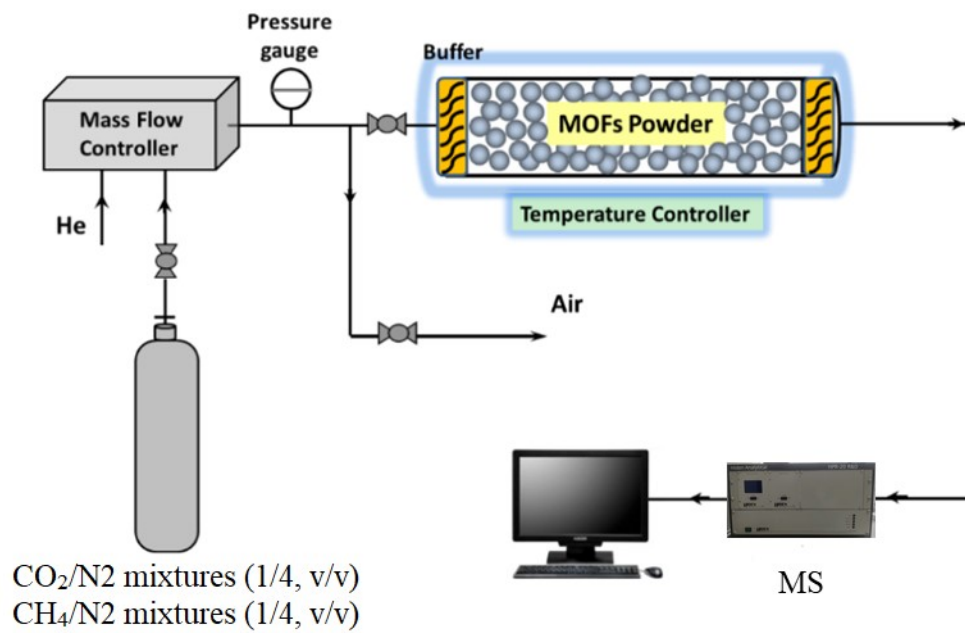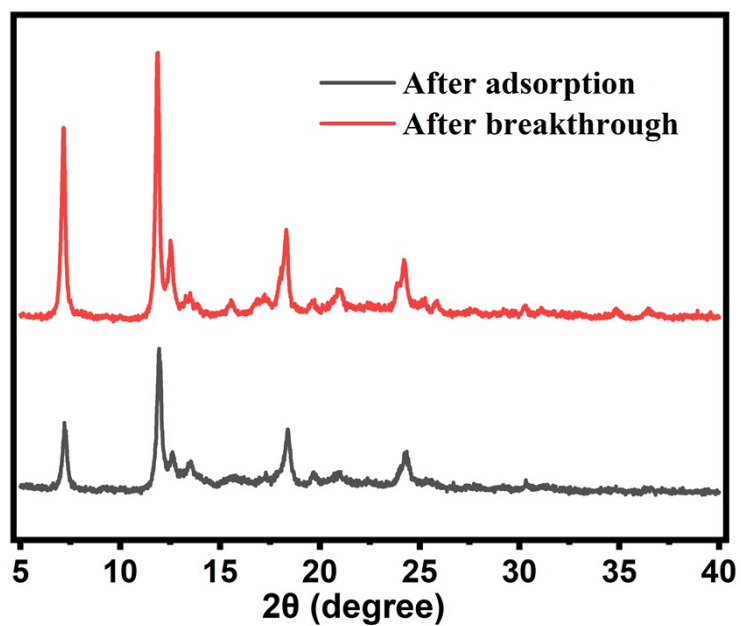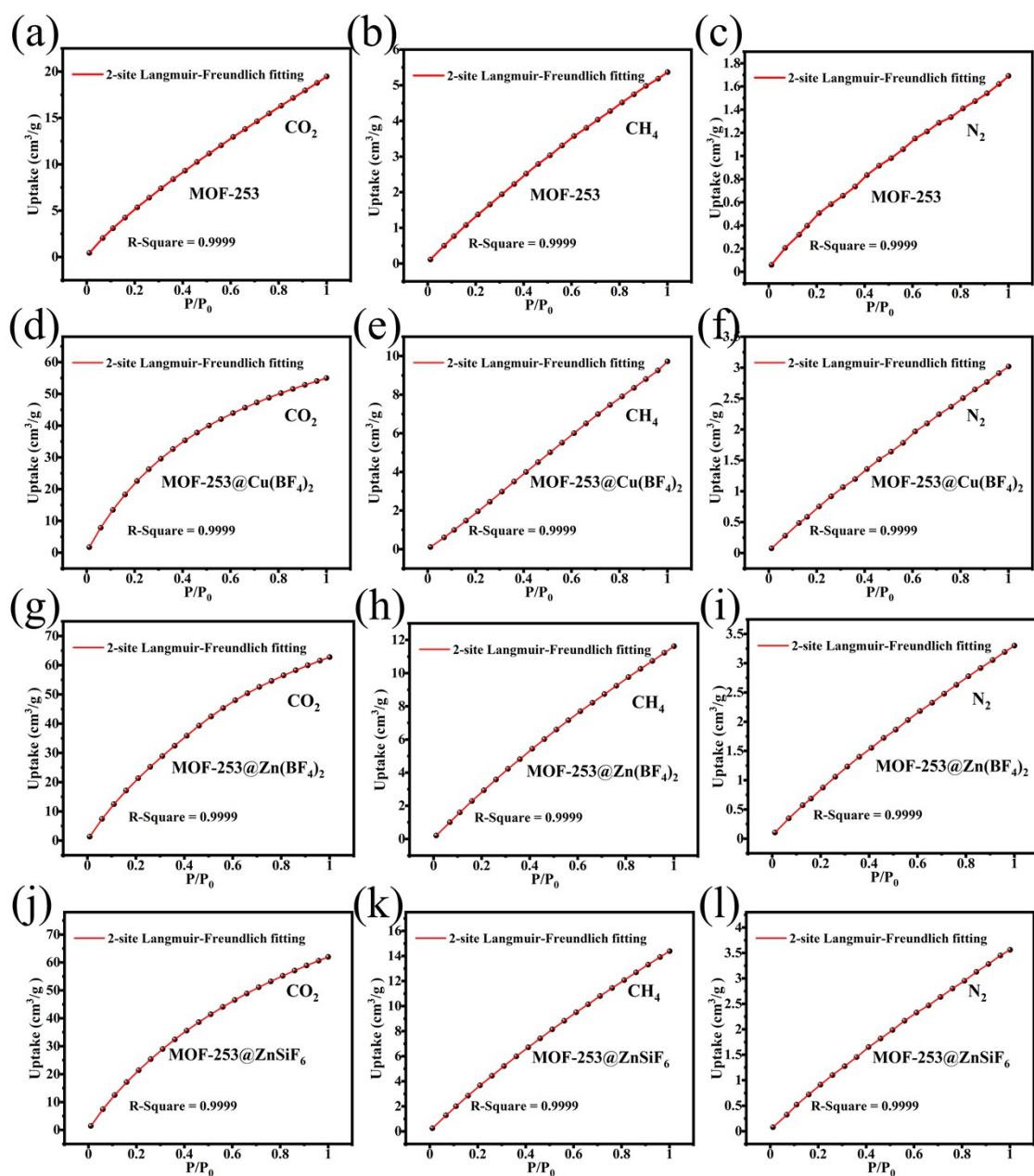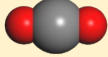|	Structure	Molecular size ($Å^3$)	Kinetic diameter (Å)	Boiling point (K)	Polarizability ($\times 10^{-25}/cm^3$)	Quadrupole moment ($\times 10^{26}/esu\ cm^2$)
CO_2		$3.18 \times 3.33 \times 5.36$	3.3	194.7	29.11	-4.30
CH_4		$3.7 \times 3.7 \times 3.7$	3.758	111.66	25.93	0
N_2		$3.6 \times 3.6 \times 3.6$	3.64	77.35	17.403	1.52

Table S2 EDS element content analysis for MOF-253, MOF-253@Cu(BF$_4$)$_2$, MOF-253@Zn(BF$_4$)$_2$ and MOF-253@ZnSiF$_6$.

Adsorbents	Al (wt.%)	N (wt.%)	Cu (wt.%)	Zn (wt.%)	F (wt.%)
MOF-253	53.230	46.770	-	-	-
MOF-253@Cu(BF$_4$)$_2$	17.490	17.984	33.640	-	30.886
MOF-253@Zn(BF$_4$)$_2$	16.523	15.768	-	38.332	29.377
MOF-253@ZnSiF$_6$	17.646	16.160	-	41.324	22.854

Table S3 ICP metals content analysis for MOF-253, MOF-253@Cu(BF$_4$)$_2$, MOF-253@Zn(BF$_4$)$_2$ and MOF-253@ZnSiF$_6$.

Adsorbents	Al (wt.%)	Cu (wt.%)	Zn (wt.%)
MOF-253	17.1	-	-
MOF-253@Cu(BF$_4$)$_2$	15.7	17.7	-
MOF-253@Zn(BF$_4$)$_2$	13.9	-	12.0
MOF-253@ZnSiF$_6$	12.8	-	15.7

Table S4 Adsorption capacity of MOF-253@ZnSiF$_6$ in equilibrium and dynamic conditions.

	Equilibrium adsorption (1 bar)	Breakthrough experiments (CO$_2$/N$_2$ or CH$_4$/N$_2$, 1/4)
CO$_2$ (cm^3/g)	61.9	16.1
CH$_4$ (cm^3/g)	14.4	4.2

Table S5 Summary of the equilibrium uptakes, CO_2/N_2 uptake ratio in some reported MOFs

Adsorbents	CO_2 uptake (cm³/g)	N_2 uptake (cm³/g)	CO_2/N_2 uptake ratio	Reference
MOF-253	19.48	1.69	11.5	This work
MOF-253@Cu(BF$_4$)$_2$	54.96	3.02	18.1	This work
MOF-253@Zn(BF$_4$)$_2$	62.7	3.3	19	This work
MOF-253@ZnSiF$_6$	61.95	3.5	17.7	This work
In(aip)$_2$	28.1	0.2	140.5	[1]
UTSA-280	67.3	6	11.2	[2]
NJUBai35	72.8	4	18.2	[3]
Cu-Fpymo	39.2	0.33	118	[4]
NKMOF-9a	46.4	2.2	21.1	[5]
MUV-26α	33.15	0.56	59.2	[6]
FJUT-3	51	5	10.2	[7]
FJUT-4	23.5	1.3	18.1	[8]

Table S6 Summary of the equilibrium uptakes, CH_4/N_2 uptake ratio in some reported MOFs

Adsorbents	CH_4 uptake (cm^3/g)	N_2 uptake (cm^3/g)	CH_4/N_2 uptake ratio	Reference
MOF-253	5.36	1.69	3.2	This work
MOF-253@Cu(BF$_4$)$_2$	9.72	3.02	3.2	This work
MOF-253@Zn(BF$_4$)$_2$	11.62	3.3	3.5	This work
MOF-253@ZnSiF$_6$	14.39	3.5	4.1	This work
Al-BPDC	5.90	2.70	2.2	[9]
Al-NDC	10.86	3.39	3.2	[9]
Al-BDC	15.98	5.06	3.1	[9]
Al-FUM-Me	27.19	5.18	5.2	[9]
Al-CDC	32.1	5.1	6.3	[10]
Al-FUM	20.44	5.15	3.9	[11]
MIL-53(Al)	5.21	4.35	1.2	[12]

Table S7 Dual-Langmuir-Freundlich fitting parameters for CO_2, CH_4 and N_2 in MOF-253 at 298 K.

	Site A			Site B		
	$q_{A,sat}$	b_A	v_A	$q_{B,sat}$	b_B	v_B
	$cm^3\ g^{-1}$	bar^{-1}	dimensionless	$cm^3\ g^{-1}$	bar^{-1}	dimensionless
CO_2	305.34	0.07	0.85	0.55	0.47	6.60
CH_4	24.49	0.26	1.05	0.26	4.92	0.65
N_2	0.04	77.46	114.08	17.01	0.11	0.83

Table S8 Dual-Langmuir-Freundlich fitting parameters for CO_2, CH_4 and N_2 in MOF-253@Cu(BF$_4$)$_2$ at 298 K.

	Site A			Site B		
	$q_{A,sat}$	b_A	v_A	$q_{B,sat}$	b_B	v_B
	$cm^3\ g^{-1}$	bar^{-1}	dimensionless	$cm^3\ g^{-1}$	bar^{-1}	dimensionless
CO_2	0.59	1.15	11.03	89.03	1.59	0.99
CH_4	1.48	2.08	2.32	61.63	0.16	1.05
N_2	8.45	0.26	1.43	3.39	0.59	0.77

Table S9 Dual-Langmuir-Freundlich fitting parameters for CO_2, CH_4 and N_2 in MOF-253@Zn(BF$_4$)$_2$ at 298 K.

	Site A			Site B		
	$q_{A,sat}$	b_A	v_A	$q_{B,sat}$	b_B	v_B
	cm^3 g^{-1}	bar^{-1}	dimensionless	cm^3 g^{-1}	bar^{-1}	dimensionless
CO_2	123.76	0.92	0.95	3.42	93.88	6.23
CH_4	13.12	0.01	11.11	60.67	0.23	0.97
N_2	23.92	0.16	0.90	0.09	7.48	8.18

Table S10 Dual-Langmuir-Freundlich fitting parameters for CO_2, CH_4 and N_2 in MOF-253@ZnSiF$_6$ at 298 K.

	Site A			Site B		
	$q_{A,sat}$	b_A	v_A	$q_{B,sat}$	b_B	v_B
	cm^3 g^{-1}	bar^{-1}	dimensionless	cm^3 g^{-1}	bar^{-1}	dimensionless
CO_2	0.65	13.25	3.28	140.57	0.77	0.94
CH_4	0.04	20.92	28.79	95.41	0.18	0.95
N_2	0.04	35.56	25.30	39.09	0.10	0.91

References

[1] Y.-M. Gu, H.-F. Qi, S. Qadir, T.-J. Sun, R. Wei, S.-S. Zhao, X.-W. Liu, Z. Lai, S.-D. Wang, *Chem. Eng. J.*, 2022, **449**, 137768.

[2] R.-B. Lin, L. Li, A. Alsalme, B. Chen, *Small Struct.*, 2020, **1**, 2000022.

[3] J. Jiang, Z. Lu, M. Zhang, J. Duan, W. Zhang, Y. Pan, J. Bai, *J. Am. Chem. Soc.*, 2018, **140**, 17825-17829.

[4] Y. Shi, Y. Xie, H. Cui, Z.A. Alothman, O. Alduhaish, R.-B. Lin, B. Chen, *Chem. Eng. J.*, 2022, **446**, 137101.

[5] S. Geng, H. Xu, C.-S. Cao, T. Pham, B. Zhao, Z. Zhang, *Angew. Chem. Int. Ed.*, 2023, **62**, e202305390.

[6] I. Abanades Lazaro, E.C. Mazarakioti, E. Andres-Garcia, B.J.C. Vieira, J.C. Waerenborgh, I.J. Vitorica-Yrezabal, M. Gimenez-Marques, G. Minguez Espallargas, *J. Mater. Chem. A*, 2023, **11**, 5320-5327.

[7] L. Zhang, Z. He, Y. Liu, J. You, L. Lin, J. Jia, S. Chen, N. Hua, L.A. Ma, X. Ye, Y. Liu, C.X. Chen, Q. Wang, *ACS Appl Mater Interfaces*, 2023, **15**, 30394-30401.

[8] L. Zhang, S. Lin, Y. Liu, X. Zeng, J. You, T. Xiao, Y. Feng, Z. He, S. Chen, N. Hua, X. Ye, Z.-W. Wei, C.-X. Chen, *Inorg. Chem.*, 2023, **62**, 8058-8063.

[9] M. Chang, T. Yan, Y. Wei, J.-X. Wang, D. Liu, J.-F. Chen, ACS Appl. Mater. Interfaces, 2022, **14**, 25374-25384.

[10] M. Chang, Y. Zhao, D. Liu, J. Yang, J. Li, C. Zhong, *Sustainable Energy Fuels*, 2020, **4**, 138-142.

[11] H. Zhenghui, H. Peng, L. Jia, S. Fang, Z. Youquan, C. Kungang, Y. Yunpan, K.

Chengjun, Z. Zhaoqiang, J. Hongbing, *Sep. Purif. Technol.*, 2022, **286**, 120446.

[12] A. Pereira, A.F.P. Ferreira, A. Rodrigues, A.M. Ribeiro, M.J. Regufe, *Microporous Mesoporous Mater.*, 2022, **331**, 111648.